Hindawi
Advances in Civil Engineering
Volume 2020, Article ID 8868140, 23 pages
https://doi.org/10.1155/2020/8868140

Research Article

Effects of Different Conditions of Water Cooling at High Temperature on the Tensile Strength and Split Surface Roughness Characteristics of Hot Dry Rock

Hanbo Cui, Jupeng Tang, and Xintong Jiang

School of Mechanics and Engineering, Liaoning Technical University, Fuxin, Liaoning 123000, China

Correspondence should be addressed to Jupeng Tang; tangjupeng@lntu.edu.cn

Received 23 September 2020; Revised 30 October 2020; Accepted 7 November 2020; Published 25 November 2020

Academic Editor: Zhi Cheng Tang

To investigate the effects of the different conditions of water cooling at high temperature on the tensile strength and split surface roughness characteristics of hot dry rock in the Songliao Basin, the physical characteristics, tensile strength, and split surface roughness of granite under different conditions of water cooling at high temperature were studied. In addition, the relationship between tensile strength and split surface roughness under different conditions of water cooling at high temperature was established. The results showed the following: (1) as the rock temperature increased, the number of water injection cycles increased or the water injection temperature decreased, the mechanical properties of the specimen weakened, and the roughness of the split surface increased. The threshold for the effect of the rock temperature on the split surface roughness of granite was 300°C. At 400°C, the tensile strength greatly decreased. At 600°C, the tensile strength, height mean square error (MSE), fluctuation difference, roughness coefficient, and roughness profile index of the specimen were 0.21, 2.51, 2.57, 8.92, and 1.06 times those at 100°C, respectively. After five heating-cooling cycles, the tensile strength, height MSE, fluctuation difference, roughness coefficient, and roughness profile index of the specimen were 0.57, 1.33, 1.49, 1.29, and 1.01 times those after one cycle, respectively. (2) The roughness angle calculated using the root mean square of the first derivative of the profile was always greater than that derived using the roughness profile index. In addition, the higher the temperature, the lower the water temperature, the more high-temperature-water cooling cycles, the greater the difference between the above two calculations. (3) When the tensile strength varies, the factors affecting the variation in the height MSE and surface roughness were in the following descending order: rock temperature, number of heating-cooling cycles, and water temperature. In addition, the higher the tensile strength, the lower the roughness coefficient. This study is expected to provide a reference for the selection of different conditions of water cooling at high temperature for thermal recovery in the Songliao Basin.

1. Introduction

The enhanced geothermal system (EGS) is a technology used for the development of hot dry rock (HDR) by fracturing a reservoir via artificial fracturing and extracting the heat for use from the heat exchange between water and HDR (MIT [1]). The HDR temperature is the primary factor in selecting the location of EGS thermal recovery and determining the production prospects and operating cost of the target area. As water acts as a heat transmission fluid, water temperature is an important control parameter for thermal recovery. The number of water injection circulation cycles at high temperatures is also closely related to the lifespan of a reservoir. Therefore, understanding the relationships between the temperature of the target area, the water injection temperature, and the number of water circulation cycles performed at high temperatures with the physical and mechanical properties of granite, which are important for the high-quality production of the EGS, is valuable.

In recent years, many numerical simulations have studied the relationship between the injection-production conditions and EGS. Jing et al. [2], Vogt et al. [3], and Zhao et al. [4] discovered that the initial temperature of a reservoir is closely related to the EGS production capacity, and the

higher the temperature is, the better the heat production efficiency is. With the development of thermal recovery, when the temperature of the reservoir decreases to a certain level, the production capacity also decreases. Xin et al. [5] found that the fracture number, fracture bifurcation, and fracture connectivity of the fracturing area determine the final temperature production, net power generation, and thermal recovery rate. Fox et al. [6] and Kazemi et al. [7] demonstrated that as the production capacity decreased, the heat production efficiency was significantly reduced; production should be stopped until the heat energy is restored; and HDR experienced multiple cycles of water cooling at high temperatures during this period. Bataillé et al. [8] and Gong et al. [9] noted a certain correlation between the temperature of the injected fluid and the production capacity. Some researchers have experimentally investigated the physical and mechanical properties of rock in high temperature conditions. Gautam et al. [10] conducted uniaxial tensile and microscopic tests of granite after naturally cooling from high temperatures and established the relationship between the thermal damage and the tensile strength. Shen et al. [11, 12] performed a cooling shock treatment on perforated granite using a calcium chloride solution. They found that when the temperature was above 550°C, as the fluid was injected, obvious macrofractures appeared around the injection hole of the rock, and the lower the refrigerant temperature, the more pronounced the macrofractures. In addition, the higher the rock temperature, the greater the drop in the wave velocity, apparent resistivity, and peak stress. Hu et al. [13] explored the fracture characteristics of granite subjected to tensile failure using different cooling methods. Isaka et al. [14] investigated the mechanical properties of granite under natural cooling and water cooling and found that the deterioration of the rock under water cooling was much higher than that under natural cooling. Zhao [15] noted that at real-time high temperatures, the tensile strength of granite decreases with increasing temperatures. Li and Ju [16] conducted tests on the mechanical properties of granite after several thermal cycles and discovered that most of the mechanical property loss of granite after high-temperature cycles occurred within five thermal cycles. Hosseini [17] found that as the number of high temperature natural cooling cycles increased, the longitudinal wave velocity and tensile strength of the rock decreased significantly.

In addition, some researchers have investigated rock roughness and discussed the correlations between the roughness and the mechanical properties. Ficker [18] evaluated the rock surface roughness using the root mean square (RMS) height. Zeng et al. [19] determined that tensile fracture was a main component of fractures in low-permeability reservoirs. Grasselli and Egger [20] investigated the relationship between the joint roughness coefficient (JRC) and the tensile fracture propagation pattern. Zhang et al. [21] qualitatively examined the relationship between the tensile strength of split granite and the roughness of the split surface. Diaz et al. [22] suggested that the fracture roughness affects the heat production efficiency of an EGS. Tang and Zhang [23] applied shear tests to simulate the internal fracture structure of a deep, high-temperature rock body to explore the relationship between the temperature and surface roughness of a specimen. Li et al. [24] found that the roughness of the rock surface will affect the liquid nitrogen cryogenic quenching process. Tang et al. [23, 25–27] conducted uniaxial compression tests and shear tests on rocks after heat treatment at 20–800°C and analyzed the effects on several key parameters. As the temperature rises, the concerning parameters exhibit different change rules: the basic friction angle, the uniaxial compressive strength, and the joint roughness coefficient of granite decrease nonlinearly; the cohesion and internal friction angle exhibit a reverse *S*-shape changing trend; the peak shear strength increases linearly below 400°C and decreases nonlinearly at 400–800°C. The changing of rock mechanical properties and joint surface roughness parameters is related to the dehydration process and the uneven expansion of mineral grains. It is also pointed out [27] that the three-point peak criterion is the most suitable evaluation standard for rock joints.

Numerical simulations of EGS thermal recovery have mainly been performed to study the heat production efficiency, and the investigation of high-temperature granite has focussed on the physical and mechanical properties of rock after natural cooling or at real-time high temperatures. However, there are few studies on the effects of water cooling at high temperatures or cyclic water cooling at high temperatures on the physical and mechanical properties of rock using HDR as the research substrate. In addition, many tensile fractures usually form in low-permeability strata during the thermal recovery process. Different conditions of water cooling at high temperature can cause large differences in the roughness of a fracture surface, which affects the flow path and heat transfer process and changes the heat production efficiency.

Currently, optical and mechanical methods exist for measuring the roughness of a structural surface. The optical methods consist of a laser transmitter–receiver and a digital simulation system, which can measure the three-dimensional (3D) spatial morphology of a structural surface. Although the optical method has a high measurement speed and accuracy, its shortcomings include a small measurement range of the height difference and a very high cost, which limit it to measuring laboratory-fixed specimens within a short distance. The mechanical method consists of a contact probe, driving device, and digital simulation system, which can only be employed for two-dimensional measurements. The application range of the mechanical method is also limited to laboratory-fixed specimens. Therefore, building a low-cost, flexible, and accurate instrument for 3D roughness measurements is necessary.

Based on the above factors, to investigate the effects of different conditions of water cooling at high temperature on the physical and mechanical properties as well as the roughness characteristics of the split surface of HDR, we employed HDR production in the Songliao Basin as the research background to conduct a Brazilian disc test on specimens under different conditions of water cooling at high temperature. A self-developed roughness profilometer was used to measure the roughness of the split surface to

study the effects of the rock temperature, water temperature, and number of heating-cooling cycles performed on the physical characteristics (apparent morphology and mass loss rate), mechanical properties (tensile strength), and split surface roughness properties (height difference parameters, including the height mean square error (MSE) and fluctuation difference, and texture parameters, including the roughness coefficient, roughness profile index, and roughness angle). We have established a relationship between the mechanical parameters and roughness coefficient (tensile strength-height MSE and tensile strength-roughness coefficient) of different conditions of water cooling at high temperature. This study can provide a reference for the selection of different conditions of water cooling at high temperature at the geothermal field in the Songliao Basin.

2. Overview of the Tests

2.1. Geological Background. The Songliao Basin spans Inner Mongolia, Heilongjiang, Jilin, and Liaoning. Under the influence of geological tectonic movements, faults at the basin basement notably developed, and there is frequent volcanic activity, as well as multiple geothermal anomalies (Zhang et al. [28]). Three main types of heat sources exist in the geothermal field: mantle convection, magma intrusion, and the decay of radioactive elements inside the rock mass. Under the combined action of the three sources, the geothermal flux is in the range of 51.5–90.0 mW/m^2. The average geothermal gradient is 5.7°C/100 m. The total amount of HDR resources is 0.62×10^6 g/cm^3 EJ (Li [29]). The upper part of the target stratum is mainly composed of epimetamorphic rock series and granite, and the lower part is mainly composed of hypometamorphic rock series and gneissic granite. The overlying mudstone caprocks can ensure the storage of thermal energy, and the Songhua River system is located near a geothermal field. Based on these factors, the geothermal field in the Songliao Basin has reasonable prospects for geothermal development.

2.2. Specimen Preparation. The northern Songliao Basin was selected as the target area for sampling. The specimens appeared to be greyish white with a density between 2.71 g/cm^3 and 2.99 g/cm^3. The main mineral compositions include quartz, black or white mica, potash feldspar, plagioclase, pyroxene, and hornblende, as shown in Table 1. A coring machine, cutting machine, and grinding machine were used to machine and polish the specimens. The specimen dimensions were ϕ50 mm × 25 mm with height and diameter errors of <3 mm. A total of 16 sets of tests were performed, and each set included three specimens.

2.3. Test Design. Table 2 shows the design of the tests.

(1) Different heating temperatures: the HDR was dense, impermeable high-temperature rock buried at a depth of 3–10 km. The rock body contained no water or water vapour, and the temperature was often in the range of 150–650°C (Zhao et al. [4]). Based on current research findings (Zhang et al. [30], Zhao et al. [31], Zhang et al. [32], and Yang et al. [33]) and the future development of HDR, the specimens were heated to 100°C, 200°C, 300°C, 400°C, 500°C, or 600°C. That is, the heating temperature was 100–600°C, the water temperature was 20°C, and one water cooling cycle was performed at a high temperature.

(2) Different water temperatures: the water temperature of the Songhua River ranges between 1°C and 25°C. Considering the rise in the water temperature during injection, water temperatures of 1°C, 20°C, 40°C, 60°C, and 80°C were selected for the test. That is, the water temperature was 1–80°C, the specimen temperature was 300°C, and one water cooling cycle was performed at a high temperature.

(3) The number of heating-cooling cycles: considering the number of cycles of water injection and heat recovery, the number of water cooling cycles at high temperatures was one, two, three, four, or five. That is, the number of heating-cooling cycles was 1–5 (Fox et al. [6] and Li and Ju [16]), the specimen temperature was 300°C, and the water temperature was 20°C.

The test contents included the cyclic water cooling at a high temperature test, the Brazilian disc test, and the roughness test. Following the "Regulation for Testing the Physical and Mechanical Properties of Rock" [34], adjustments were made according to the test conditions. The test process is shown in Figure 1.

(1) Measurement of specimens in the natural state: a balance was used to measure the mass, and a Vernier caliper was used to measure the height and diameter.

(2) Heating and water cooling processes under different test protocols, specifically shown in Figures 2(a) and 2(b).

   (a) Different heating temperatures: an electric stove was used to heat the specimens to the set temperatures (100–600°C) at a rate of 30°C/min. To ensure even heating inside and outside the specimen, the specimens were kept at a constant temperature for 4 h (Yan et al. [35]) and then placed in an alkali aggregate reaction chamber and water-cooled for 4 h (at a water temperature of 20°C, the test showed that, after water cooling for 4 h, the temperatures of the specimens all decreased to approximately 20°C, indicating that no more heat transferred between the water and the specimen, and the specimen was saturated).

   (b) Different water temperatures: the specimen was heated to 300°C, kept at 300°C for 4 h, and then water-cooled for 4 h (the water temperature was kept at 1–80°C).

   (c) The number of heating-cooling cycles: the specimen was kept at 300°C for 4 h and then cooled in 20°C water for 4 h. This process was repeated 1–5 times. In addition, ice was added to

Table 1: Mineral composition.

	Mineral composition				
	Quartz	Mica	Potash feldspar	Plagioclase, etc.	Pyroxene and hornblende
Colour	White transparent, etc.	Black and white, etc.	White and red, etc.	White and grey, etc.	Black and brown
Chemical composition	SiO_2, etc.	$KAI_2(ALSi_3O_{10})(OH)_2$ and Fe, etc.	$K(ALSi_3O_g)$, etc.	$Na(ALSi_3O_8)$ and $Ca(AL_2Si_2O_8)$, etc.	$(Na, Ca)_2(Mg, Fe, Al)_5$ and $[(Si, Al)_4O_{11}]_2(OH)_2$
Content (%)	26.1	8.9	36	25.2	3.8
Particle size (mm)	0.1–2.1	0.35–1.2	0.75–4	2–2.5	—
Coefficient of thermal expansion (1/°C)	5.5×10^{-7}	2.2×10^{-5}	$(5 \sim 6) \times 10^{-6}$	$(6.5 \sim 7.5) \times 10^{-6}$	—

Note. The thermal expansion coefficient of mineral composition comes from the network.

Table 2: Test scheme.

Test specimen	Heating temperature (°C)	Water temperature (°C)	The number of heating-cooling cycles (times)	Heating time (h)	Water-cooled time (h)
C1	100	20	1	4	4
C3	200	20	1	4	4
C5	300	20	1	4	4
C6	400	20	1	4	4
C7	500	20	1	4	4
C8	600	20	1	4	4
W1	300	1	1	4	4
W2	300	20	1	4	4
W3	300	40	1	4	4
W4	300	60	1	4	4
W5	300	80	1	4	4
P1	300	20	1	4	4
P2	300	20	2	4	4
P3	300	20	3	4	4
P4	300	20	4	4	4
P5	300	20	5	4	4

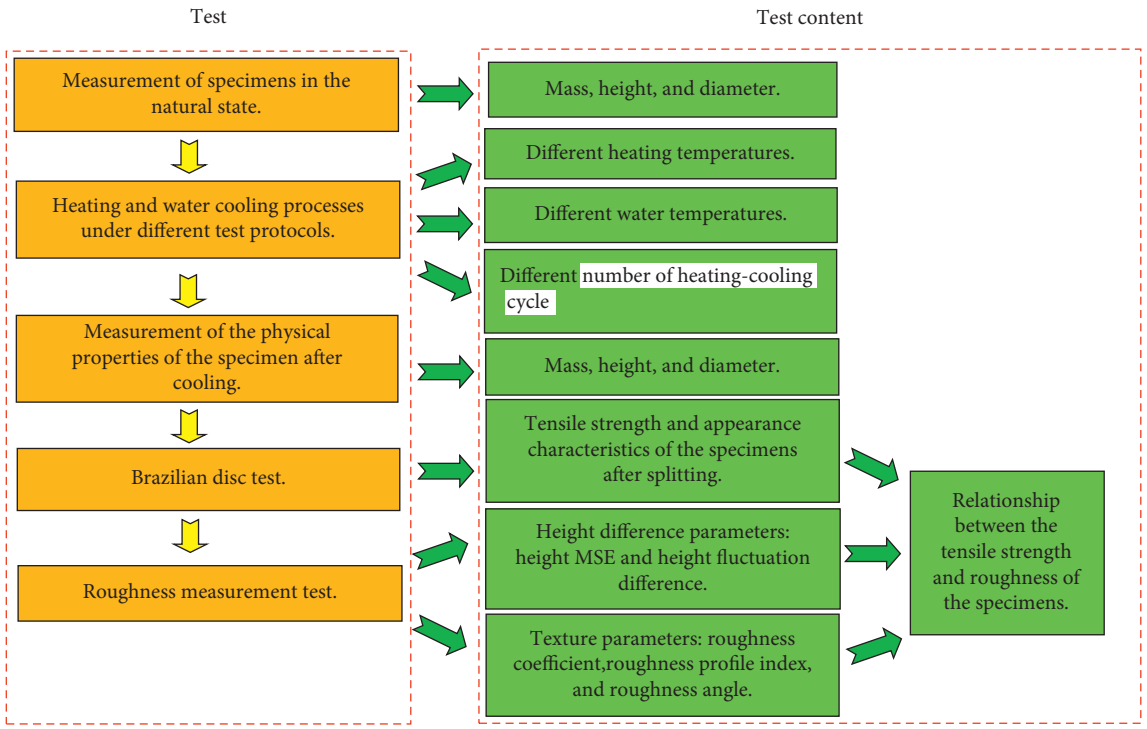

Figure 1: Test process.

cool the water to keep the water temperature consistent. An infrared thermometer was used to monitor the water temperature.

(3) Measurement of the physical properties of the specimen after cooling: the mass, height, and diameter of the specimen under different conditions of water cooling at high temperature were measured, and changes in the appearance characteristics of the specimen were observed.

(4) Brazilian disc test: thin steel wires were placed as pads on the upper and lower tension surfaces of the specimen. The specimen was then placed on a press. Experiments revealed that when the loading rate is 0.5 MPa/s, the mass loss rate is the smallest. Therefore, the test was conducted at a loading rate of 0.5 MPa/s until the specimen was damaged. The tensile strength was recorded as specifically shown in Figure 2(c).

(5) Roughness measurement test: a dial gauge was fixed on a slide rail. After it was split, the specimen was placed on the base, and the horizontal positions of the slide rail and the specimen were adjusted. The

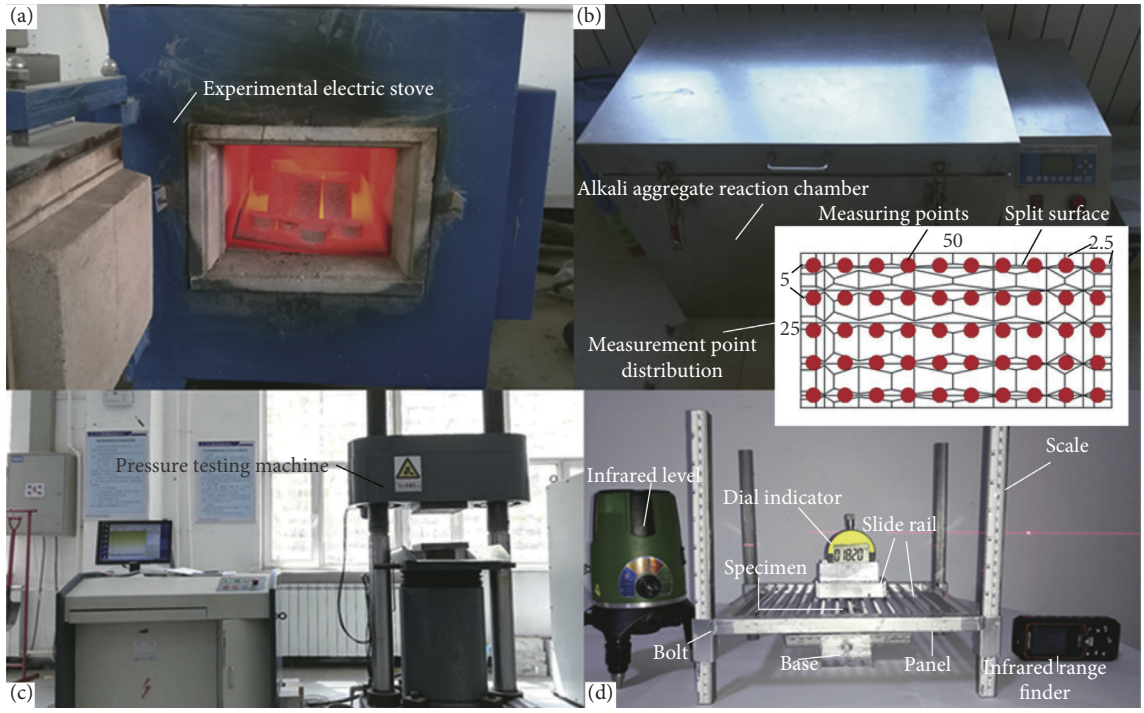

Figure 2: Test content. (a) Heating. (b) Cooling. (c) Brazilian disc test. (d) Roughness measurement.

vertical height of the panel was adjusted with nuts. The horizontal angles of the panel and the specimen were measured and levelled with an infrared level. The slide rail was pushed to perform measurements at different measuring points (an infrared range-finder was used to ensure the slide accuracy). The experiment revealed particle shredding during the splitting process. Particle shredding often occurred at the edge of the splitting surface. To minimize the effect of the side of the probe and particle shredding at the edge of the splitting surface, all shredded particles were collected and glued together. The contour sampling method was used to determine the spacing between measuring points, with the measuring points being 2.5 mm from the edge. The specific arrangement of measuring points is shown in Figure 2(d)

2.4. Test Equipment. The test equipment parameters are listed in Table 3.

2.5. Verification of the Accuracy of the Roughness Tester. To verify the accuracy of the homemade roughness tester, a portable roughness tester was used to measure each specimen. The results showed that the two testers yielded similar measurement results, indicating that the homemade tester was reliable. The verification results are shown in Figure 3.

3. Test Results and Analysis

3.1. Variation Pattern of Appearance Characteristics in Specimens under Different Conditions of Water Cooling at High Temperatures. With a temperature of 300°C or three heating-cooling cycles, the roughness of the split surface significantly increased. When the temperature reached 500°C or four heating-cooling cycles, the colour of the specimen changed significantly. Adjusting the water temperature did not notably change the appearance of the specimen.

Figures 4(a) and 4(b) show the appearance characteristics of the specimens after splitting under different conditions of water cooling at high temperature. As shown in Figure 4(a), when the temperature was between 100°C and 200°C, the appearance of the specimen changed only slightly from the natural state. The surface was greyish white with localized black spots. When the temperature was between 300°C and 400°C, the colour became lighter, and there were fewer black spots. When the temperature reached 500°C–600°C, the HDR changed from a reddish brown colour to a black-grey colour, and white crystals were locally generated. As the water temperature changed, the colour of the specimen did not change significantly. When the number of heating-cooling cycles reached four or five, the number of black spots decreased substantially, and the appearance turned from a grey-white colour to white.

Figures 4(a) and 4(b) show that all specimens had penetrating fractures in the radial direction after splitting under different conditions of water cooling at high temperature. The split surface was generally parallel to the plane defined by two thin steel wires. However, the roughness of the split surface differed. When the temperature was between 100°C and 200°C, the penetrating fractures were relatively close together. When the temperature was between 300°C and 600°C, the split surface was uneven, and even if it was pieced together, a few gaps remained. As the temperature rose, the split surface became rougher. Varying the

Table 3: Test equipment.

Function	Device	Remarks
Weighing	Electronic balance	Error 0.01 g
Heating	SX2-14-13 experimental electric stove	Room temperature to 1250°C
Cooling	JKS automatic alkali aggregate reaction chamber	1–100°C
Achieving constant temperature	101-1 electrothermal blowing dry box	Room temperature to 300°C
Brazilian disc test	YAW-microcomputer controlled electrohydraulic servopressure testing machine	Weighing range 10 t
Roughness measurement	Roughness profilometer	Micrometre (accuracy 0.001 mm) Infrared level (accuracy 0.1 mm) Infrared range finder (accuracy 0.1 mm)

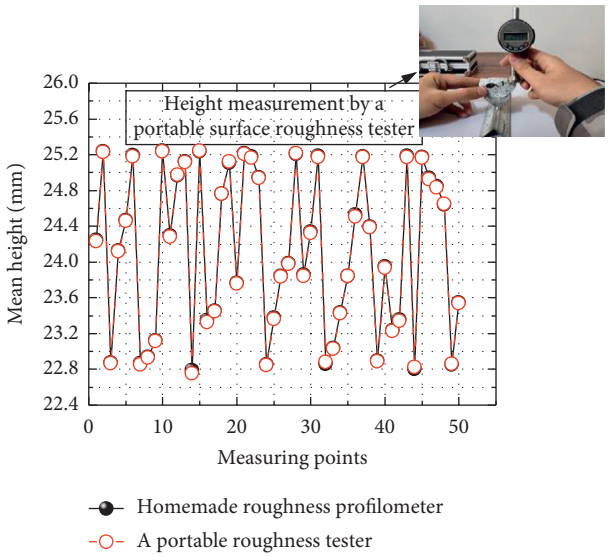

Figure 3: Verification of the accuracy of the homemade roughness tester.

water temperature did not noticeably change the roughness of the fracture surface. When the number of heating-cooling cycles went from one to two, the roughness of the fracture surface did not change significantly. After three cycles, the roughness significantly increased. Therefore, the factors that influenced the appearance characteristics of the specimens, from strongest to weakest, were the temperature of HDR, the number of water injection circulation cycles performed at high temperatures, and the water injection temperature. The different conditions of water cooling at high temperature experienced by the thermal recovery area can be deduced from the changes in the appearance characteristics.

3.2. Variation Pattern of the Mass of the Specimen under Different Conditions of Water Cooling at High Temperatures. When the temperature rose, the water temperature decreased or the number of water injection circulation cycles increased and the mass loss rate increased. When the temperature was between 300°C and 500°C or at least two water injection cycles occurred, the mass loss rate increased substantially.

To better characterize the mass change rate of the specimens subjected to different conditions of water cooling at high temperature, the mass loss rate (Q) is introduced and expressed as in the following equation.

$$Q = \frac{m_0 - m_1}{m_0} \times 100\%, \quad (1)$$

where Q is the mass loss rate (%), m_0 is the mass of the specimen in a natural state (g), and m_1 is the mass of the specimen after the test (g).

Figure 5 shows the variation pattern of the mass loss rate for the specimens under different conditions of water cooling at high temperature. An examination of the effect of temperature on the mass loss rate of the specimens indicated that the effect of a high temperature on the mass loss rate of the specimens was not significant when the temperature was between 100°C and 300°C. When the temperature reached 400°C, the mass showed a large decrease, with a loss rate of 0.2075%. At 600°C, the mass loss rate reached 0.2822%. Therefore, an increase in temperature increased the mass loss rate of the specimen.

An examination of the effect of the water temperature on the mass loss rate of specimens revealed that at a water temperature of 1°C, the mass loss rate of the specimens was approximately 0.1313%. When the water temperature reached 80°C, the mass loss rate decreased to 0.0962%. Therefore, an increase in the water temperature can reduce the mass loss of the specimens to some extent.

The effect of the number of heating-cooling cycles performed on the mass loss rate of the specimens was investigated. The mass loss of the specimen occurred mainly at the initial stage of the water injection cycle. After two heating-cooling cycles were performed, the mass loss rate of the specimen was approximately 0.1855%. As the number of water injection cycles increased, the mass loss rate of the specimen increased, but the magnitude of the loss decreased. After five cycles, the loss rate was approximately 0.2204%.

3.3. Variation Pattern of the Tensile Strength of Specimens under Different Conditions of Water Cooling at High Temperatures. When the temperature rose, the water temperature decreased or the number of water circulation cycles increased and the tensile strength of the specimen decreased. When the temperature was 400°C or at least two water

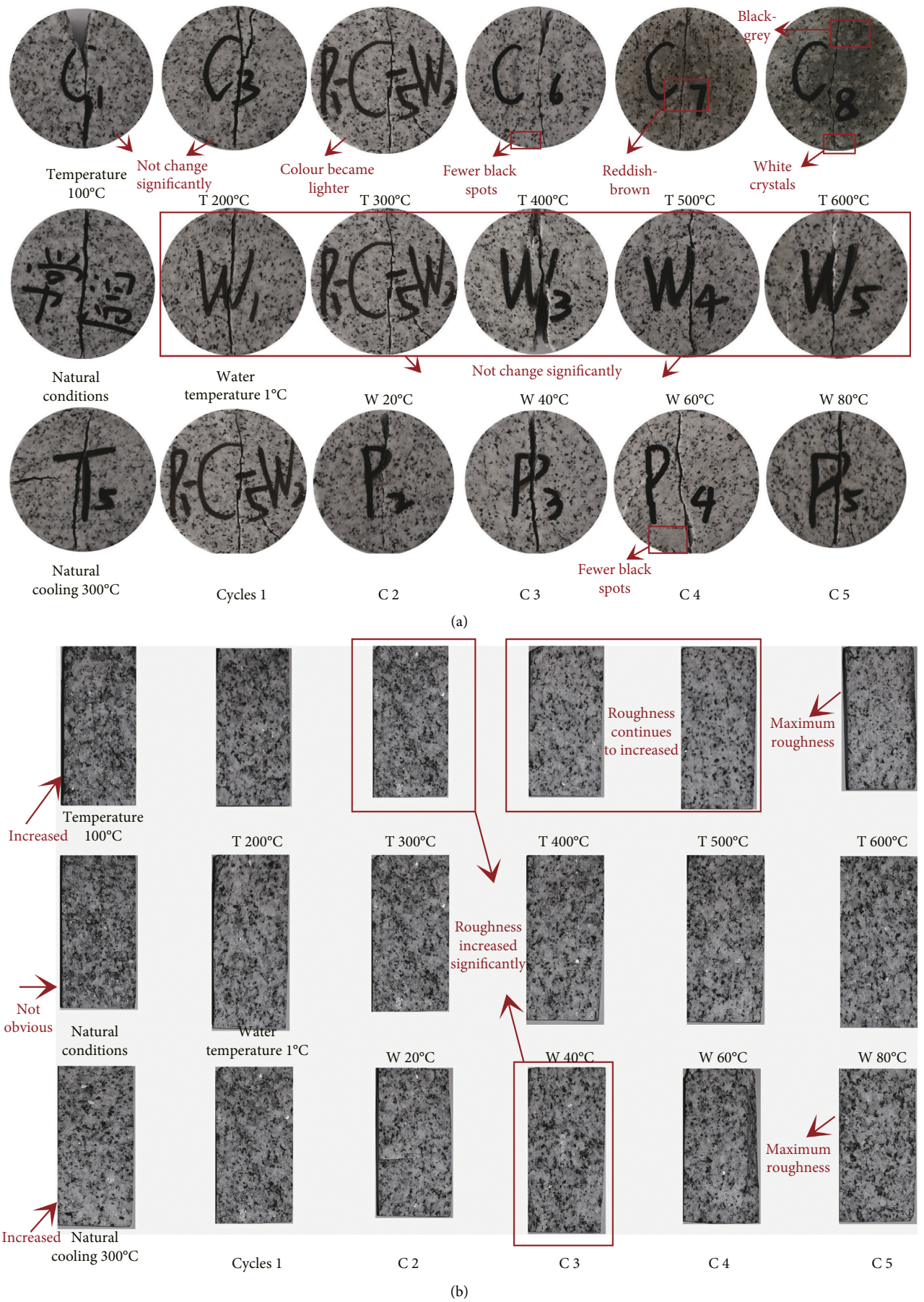

Figure 4: Appearance characteristics of the specimens after splitting under different conditions of water cooling at high temperature. (a) Front view. (b) Side view.

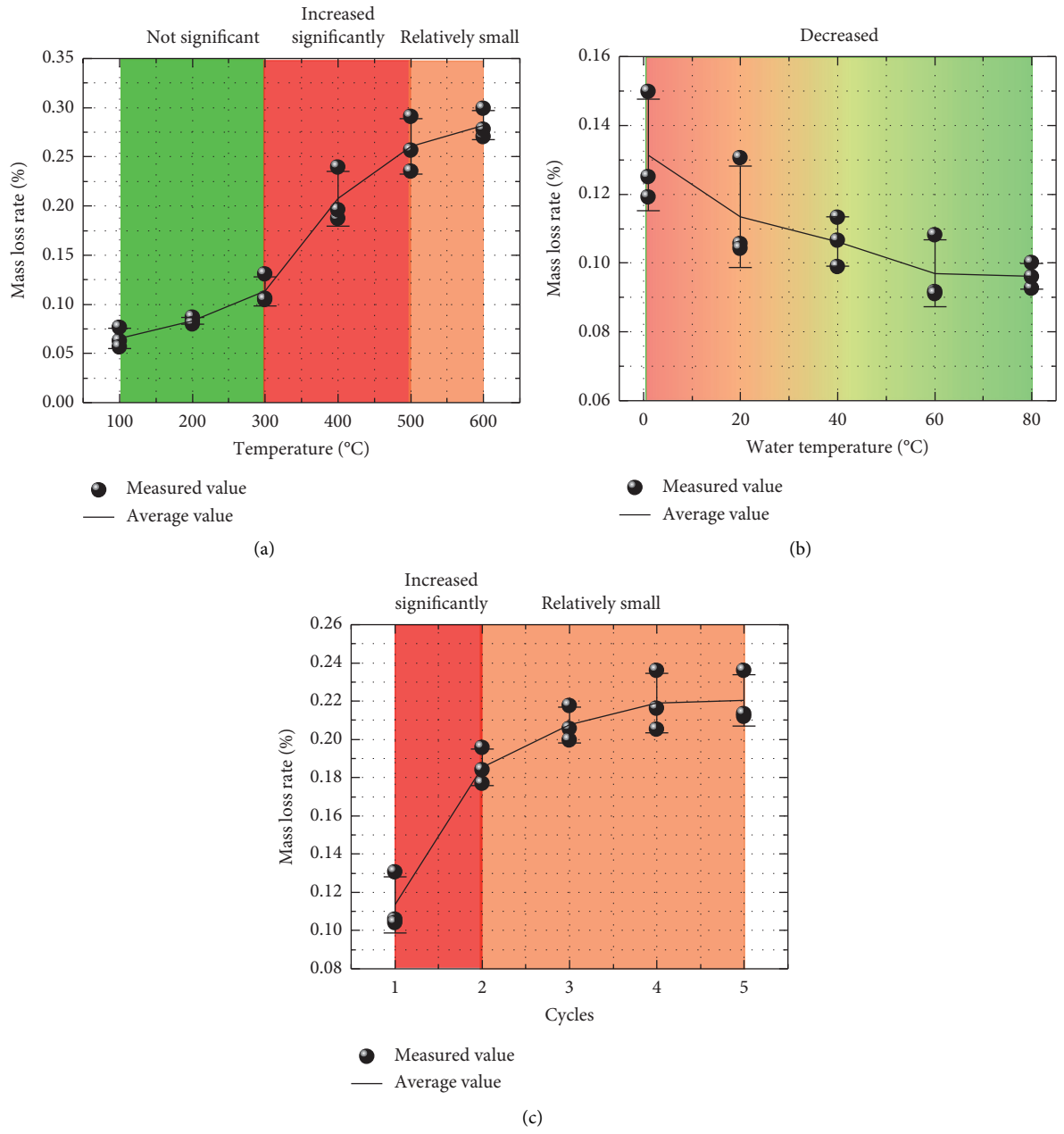

Figure 5: Mass loss rate of specimens subjected to different conditions of water cooling at high temperatures. (a) HDR temperature. (b) Water temperature. (c) The number of heating-cooling cycles.

injection cycles occurred, the tensile strength of the specimen significantly decreased.

In the thermal recovery process, many tensile fractures usually form in low-permeability strata. Note that the tensile strength (σ_t) of the specimen under different conditions of heating-cooling cycles has a certain reference value for studying the fracture initiation and propagation patterns in the target area. The tensile strength is calculated by the following equation.

$$\sigma_t = \frac{2P}{\pi dt}, \tag{2}$$

where σ_t is the tensile strength (MPa), P is the ultimate load (kN), d is the specimen diameter (mm), and t is the specimen thickness (mm).

Figure 6 shows how the tensile strength of the specimens varied under different conditions of water cooling at high temperature. An examination of the effect of temperature on the tensile strength of the specimens revealed that temperature had a relatively small effect on the tensile strength of the specimens between 100°C and 300°C. As the temperature rose, the tensile strength decreased slightly; the resulting pattern is similar to that found by Xi and Zhao [36]. At 400°C, the decrease was the most marked at 51.08%. As

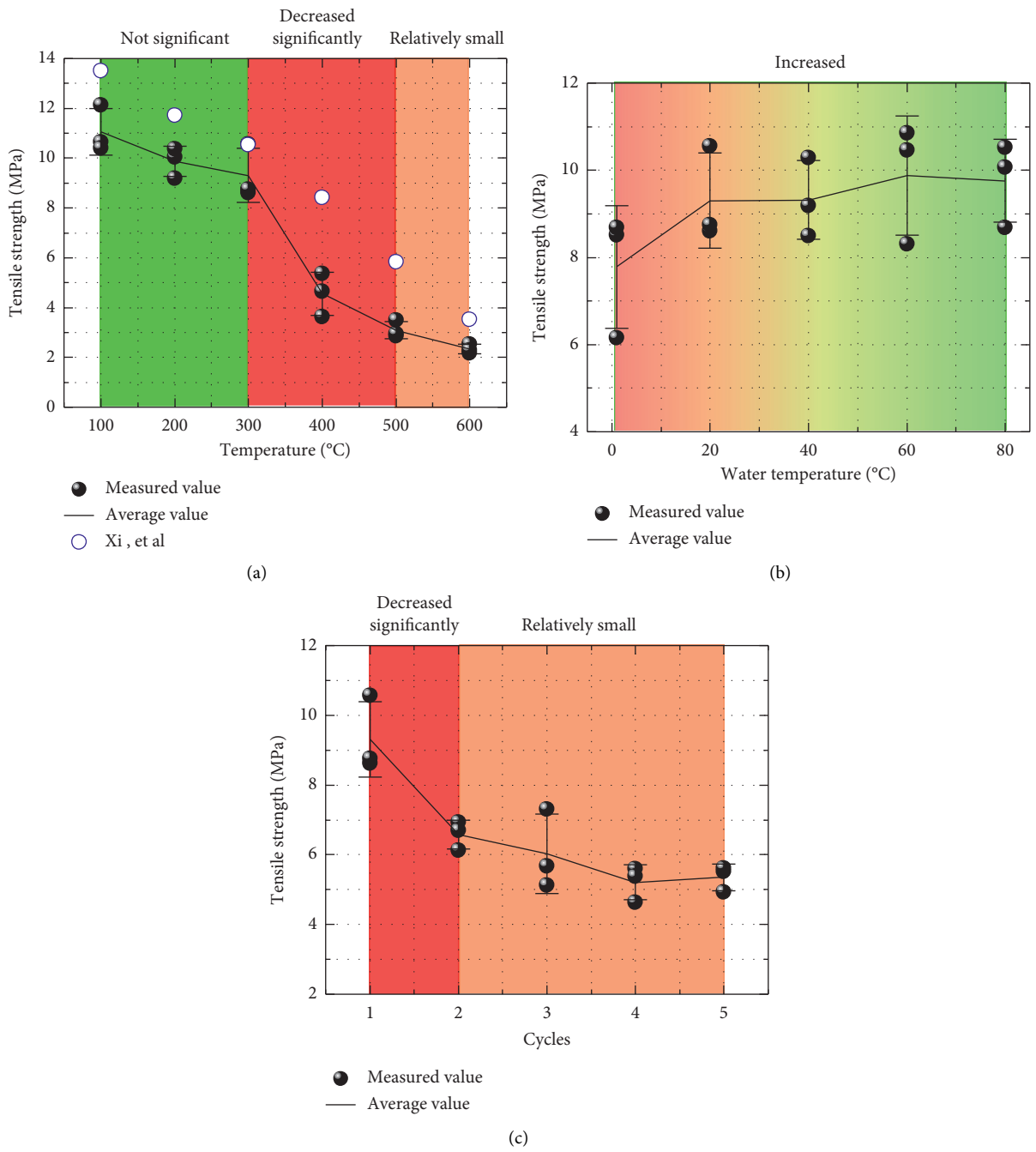

Figure 6: Tensile strength of the specimens under different conditions of water cooling at high temperatures. (a) HDR temperature. (b) Water temperature. (c) The number of heating-cooling cycles.

the temperature continued to rise, the loss slightly decelerated. At 600°C, the tensile strength of the specimen was approximately 21.27% of that at 100°C. Thus, the higher the temperature in the target area is, the lower the tensile strength of the rock mass during the water injection cooling process and the higher the possibility that tensile failure will occur.

The effect of the water temperature on the tensile strength of the specimens was examined next. At water temperatures of 1°C, 20°C, 40°C, 60°C, or 80°C, the tensile strength of the specimens was 7.78 MPa, 9.30 MPa, 9.32 MPa, 9.87 MPa, or 9.76 MPa, respectively. As the water temperature increased, the specimen tensile strength increased. Therefore, low-temperature water injection can accelerate rock fracturing.

The effect of the number of heating-cooling cycles performed on the tensile strength of the specimen was investigated. It was found that at the initial stage of high-temperature water circulation, the tensile strength decreased significantly; the decrease reached approximately 29.32% after two cycles. As the number of cycles increased, the strength loss increased. The tensile strength after five cycles

was approximately 57.47% of that after one cycle. Exposure to multiple water circulation cycles therefore raised the probability of new tensile fractures forming in the rock strata.

3.4. Variation Pattern of the Height Difference Parameters of the Specimens Subjected to Different Conditions of Water Cooling at High Temperatures. The variation pattern of the height difference parameters (the height MSE and undulation difference) of the split surfaces of the specimens for various water cooling scenarios under high temperature conditions shows that the value of each parameter increased as the temperature or the number of heating-cooling cycles increased, while the values decreased as the water temperature increased.

The height difference parameters mainly include two amplitude parameters (mean height and height MSE) and the fluctuation difference. These parameters describe the height distribution and variation characteristics of the fracture morphology and are important factors that affect the flow path of a fluid-working medium in the fracture. The amplitude parameters can reflect the uniformity of the distribution of the fluctuation pattern on the split surface, where the average height (Z_u) is expressed in equation (3), and the height MSE (Z_A) is expressed in equation (4).

$$Z_u = \frac{1}{n}\sum_{i=1}^{n} Z_i, \tag{3}$$

where Z_u is the average height (mm), n is the number of measuring points, and Z_i is the height of the ith measuring point (mm).

$$Z_A = \sqrt{\frac{1}{n-1}\sum_{i=1}^{n}\left(Z_i - Z_u\right)^2}, \tag{4}$$

where Z_A is the height MSE.

Figure 7 shows the variation pattern of the height MSE of the split surface of the specimens under different conditions of water cooling at high temperature. The effect of the HDR temperature on the height MSE of the specimen split surface was investigated first. When the temperature varied between 100°C and 200°C, the height MSE varied only slightly. As the temperature increased from 200°C to 500°C, the height MSE increased significantly. When the temperature was between 500°C and 600°C, the effect of temperature on the height MSE was smaller. The height MSE of the specimens at a high temperature of 600°C was approximately 2.51 times that at 100°C.

The effect of water temperature on the height MSE of the specimen split surfaces was investigated next. The lower the water temperature was, the larger the height MSE was. The height MSE at a water temperature of 1°C was approximately 1.22 times that at 80°C.

The effect of the number of heating-cooling cycles performed on the height MSE of the specimen split surface was also investigated. The findings revealed that as the number of heating-cooling cycles increased, the height MSE increased gradually, and the variation rate of the height MSE was relatively small for the first three cycles and increased notably, by approximately 11.39%, after four cycles. The height MSE after five cycles was 1.33 times that after one cycle.

The split surface of rock can be considered to be composed of "large" fluctuations in various regions, with a "small" roughness of these fluctuations, that is, the split surface is formed by the superposition of bumps (depressions) of different sizes. The fluctuation difference is the height difference between the relatively high bumps and the relatively low depressions. This is an important factor that affects the roughness of a split surface. The fluctuation difference between the highest bump and the lowest depression (T_Z^2) is calculated as shown in equation (5). Because choosing only one set of maximum and minimum value points would generate some randomness, we selected five high bumps and five low depression points to calculate the fluctuation difference (T_Z^{10}), as detailed in equation (6).

$$T_Z{}^2 = \left|Z_H\right| - \left|Z_C\right|, \tag{5}$$

where T_Z^2 is the fluctuation difference between the highest bump and the lowest depression (mm), Z_H is the height of the highest bump (mm), and Z_C is the height of the lowest depression (mm).

$$T_Z^{10} = \frac{1}{5}\left[\sum_{j}^{5}\left|Z_{Hj}\right| - \sum_{j}^{5}\left|Z_{Cj}\right|\right], \tag{6}$$

where T_Z^{10} is the fluctuation difference between the five bumps and five depressions (mm), Z_{Hj} is the height of the j^{th} highest bump (mm), and Z_{Cj} is the height of the j^{th} lowest depression (mm).

Figure 8 shows the variation pattern of the height fluctuation difference in the split surfaces of the specimens under different conditions of water cooling at high temperature. The effect of the rock temperature on the fluctuation difference in the split surfaces of the specimens was investigated. The height fluctuation difference approximately linearly increased with an increase in temperature. The height fluctuation difference at 600°C was approximately 2.57 times that at 100°C.

The examination of the effect of water temperature on the height fluctuation difference in the split surface of the specimens indicated that as the water temperature decreased, the height fluctuation difference gradually increased, and at 1°C, it was approximately 1.22 times that at 80°C.

The effect of the number of heating-cooling cycles performed on the height fluctuation difference of the specimen split surfaces was then investigated. As the number of cycles increased, the height fluctuation difference of the specimens gradually increased. After four cycles, the height fluctuation difference had increased significantly by approximately 17.85%. The height fluctuation difference after five cycles was approximately 1.49 times that after one cycle.

The above results indicate that the parameters of the height difference of the split surfaces were highly correlated

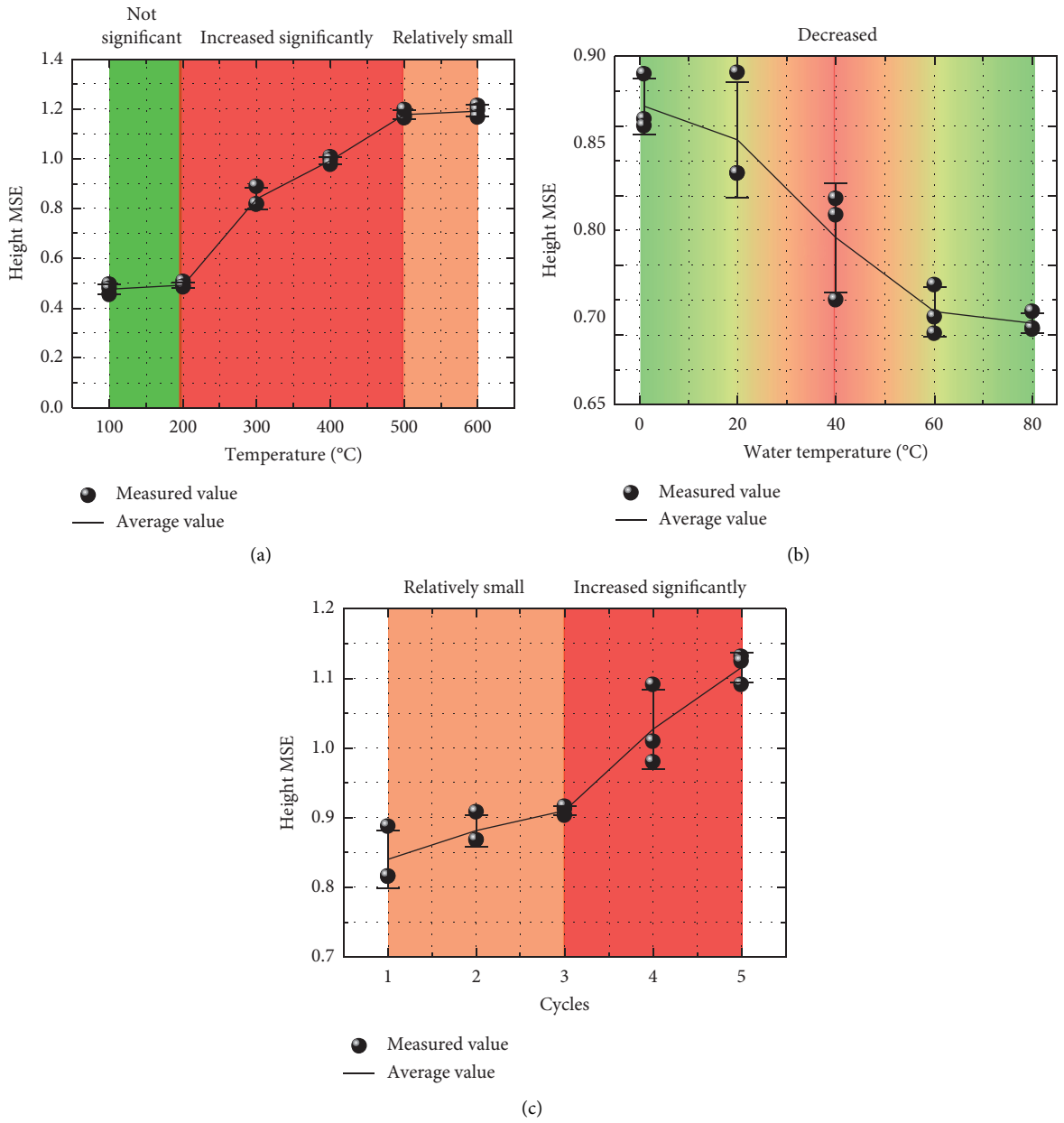

Figure 7: Height MSE of the specimen split surface under different conditions of water cooling at high temperatures. (a) HDR temperature. (b) Water temperature. (c) The number of heating-cooling cycles.

with the different conditions of water cooling at high temperature. The height MSE and fluctuation difference on the split surface increased as the rock temperature or the number of heating-cooling cycles increased, while it gradually decreased as the water temperature increased. When considering the effect of the fracture height difference parameters on thermal recovery, their effect on the flow path should be considered first. The increase in the height difference parameters will cause the formation of a few dominant seepage channels in the target rock mass. Fluid injection into these dominant paths reduces the effective heat exchange area and simultaneously causes problems, such as fluid short-circuit and flow loss, which further affect the heat production efficiency. Therefore, the effect of different conditions of water cooling at high temperature on the height difference parameters is worthy of attention.

3.5. Variation Pattern of Specimen Texture Parameters under Different Conditions of Water Cooling at High Temperatures. The variation pattern of the texture parameters (roughness coefficient, roughness profile index, and roughness angle) of the specimen split surfaces for various water cooling scenarios under high temperature conditions reveals that the values of the various texture parameters increased as the rock temperature or number of heating-cooling cycles increased, while the values slightly decreased as the water temperature increased.

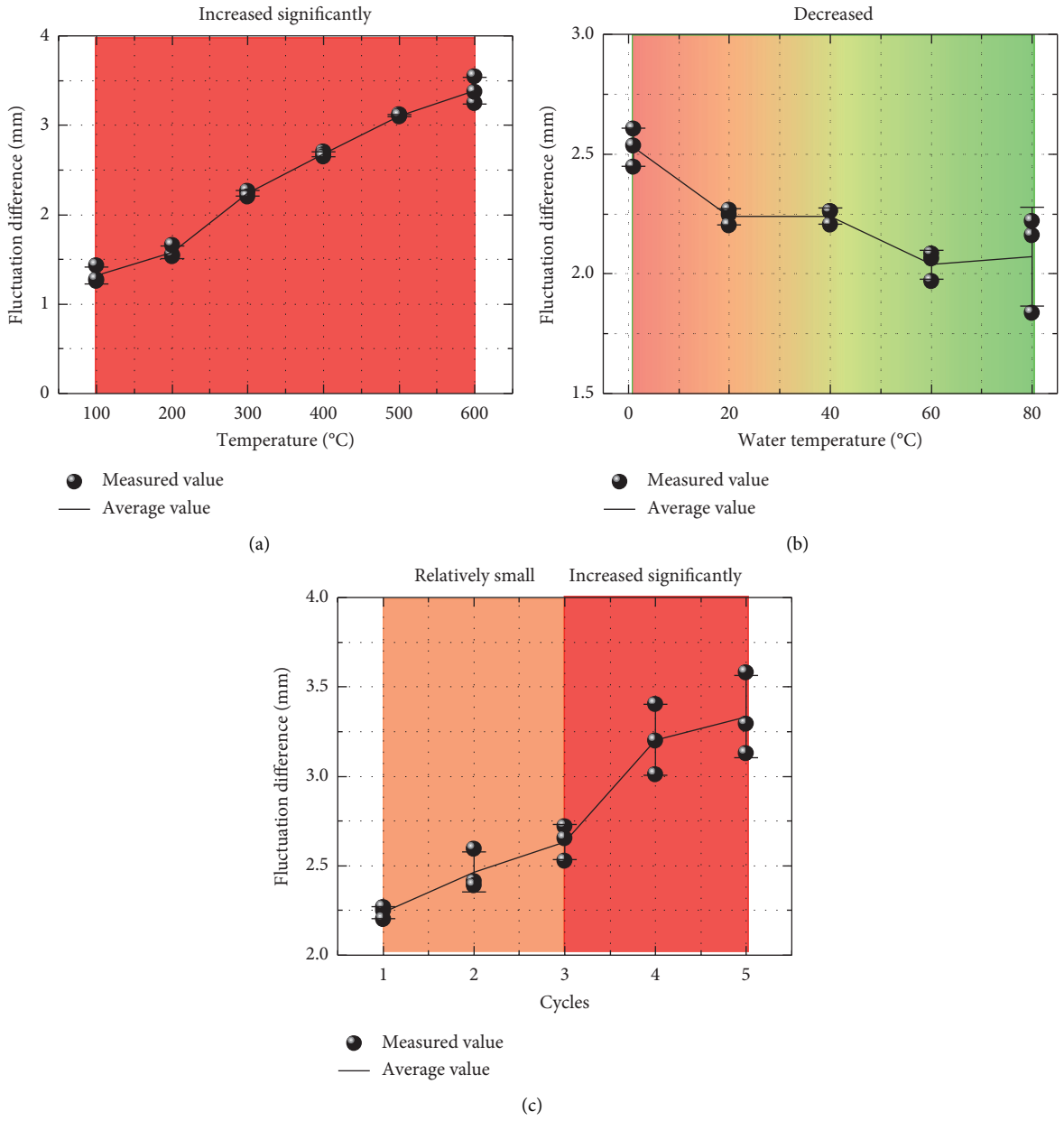

Figure 8: Height fluctuation difference in the split surfaces of specimens under different conditions of water cooling at high temperatures. (a) HDR temperature. (b) Water temperature. (c) The number of heating-cooling cycles.

The texture parameters mainly include the roughness coefficient, roughness profile index, and roughness angle, which are the statistics and statistical functions that describe the curve characteristics of the structural surface topography. In 1973, Barton [37] was the first researcher to propose the use of JRC to evaluate the roughness of the structural surface of a rock mass and successively employed the shear test, inclination test, and Brazilian disc test to calculate the roughness coefficient of a structural surface from the empirical formula. Based on Barton's 10 standard curves, we investigated the variation pattern of the roughness coefficient of a split surface under different conditions of water cooling at high temperature. The RMS of the first derivative of the profile of the split surface (Z_S) is expressed in equation (7), and the roughness coefficient of the split surface is shown in equation (8).

$$Z_s = \sqrt{\frac{\sum_i^{n-1} (Z_i - Z_{i+1})^2}{(n-1)\Delta s^2}}, \tag{7}$$

where Z_S is the RMS of the first derivative of the profile of the split surface, Z_{i+1} is the height of the $(i+1)^{\text{th}}$ measuring point (mm), and Δs is the spacing between two measuring points (mm).

$$\text{JRC} = 32.2 + 32.471 g Z_s, \tag{8}$$

where JRC is the roughness coefficient.

Figure 9 shows the variation pattern of the roughness coefficient of the specimen split surfaces under different conditions of water cooling at high temperature. The effect of the rock temperature on the roughness coefficient of the specimen split surfaces was investigated. Between 100°C and 200°C, the temperature had a minimal effect on the roughness coefficient. As the temperature rose, the roughness coefficient increased significantly at 300°C to 7.18 times that at 200°C. As the temperature continued to increase, the rate of the increase in the roughness coefficient decreased. The roughness coefficient at a high temperature of 600°C was approximately 8.92 times that at 100°C.

The effect of water temperature on the roughness coefficient of the specimen split surface was investigated next. As the water temperature decreased, the roughness coefficient gradually increased. The roughness coefficient at a water temperature of 1°C was approximately 1.57 times that at 80°C.

The effect of the number of heating-cooling cycles performed on the roughness parameters of the specimen split surfaces was then investigated. With an increasing number of cycles, the roughness coefficient of the specimen gradually increased. The roughness coefficient of the specimen with five cycles was approximately 1.29 times that with one cycle.

The ratio of the profile length to the baseline length is referred to as the roughness profile index (R_p). The roughness profile index is a quantitative parameter that uses a statistical method to characterize the roughness patterns of specimens, as shown in the following equation.

$$R_P \approx \frac{\sum_{i=1}^{n-1} \sqrt{\Delta s^2 + \left(Z_i - Z_{i+1}\right)^2}}{\Delta s\,(n-1)}, \tag{9}$$

where R_P is the roughness profile index.

Figure 10 shows the variation pattern of the roughness profile index of the specimen split surfaces under various water cooling at high temperature conditions. An examination of the effect of rock temperature on the roughness profile index of the specimen split surfaces revealed that at temperatures between 100°C and 200°C, the roughness profile index varied only slightly. When the temperature reached 300°C, the roughness profile index rose significantly by approximately 1.88%. The roughness profile index of the specimen at a temperature of 600°C was approximately 1.06 times that at 100°C.

An examination of the effect of water temperature on the roughness profile index of the specimen split surface revealed that the roughness profile indices were 1.0241, 1.0254, 1.0177, 1.0138, and 1.0141 as the water temperature varied from 1°C to 80°C. The roughness profile index decreased slightly with an increase in water temperature.

The effect of the number of heating-cooling cycles performed on the roughness profile index of the specimen split surface was examined next. The findings revealed that as the number of water injection cycles increased, the roughness profile index increased. The roughness profile index obtained with five cycles was approximately 1.01 times that with one cycle.

The total mechanical properties of the structural surface are mainly controlled by relatively large bumps, and the inclination that characterizes a single bump on the structural surface is referred to as the roughness angle (i). The roughness angle is a commonly employed index for describing the texture characteristics of a structural surface and is a core parameter used for studying the hydraulic properties of rough fractures. The roughness angle can be obtained in terms of R_p and Z_S, as detailed in the following equations, respectively.

$$i_{R_p} = \arccos\left(\frac{1}{R_P}\right), \tag{10}$$

$$i_{Z_S} = \arctan\left(Z_S\right), \tag{11}$$

where i_{R_p} is the roughness angle obtained in terms of R_P (°), and i_{Z_S} is the roughness angle obtained in terms of Z_S (°).

The variation pattern of the roughness angle was the same as the variation patterns of the roughness coefficient and roughness profile index. Figure 11 shows the variation pattern of the roughness angle of the specimen split surface under different conditions of water cooling at high temperature. The effect of rock temperature on the roughness angle of the specimen split surface was investigated first. The findings indicate that the roughness angle varied little at temperatures between 100°C and 200°C. When the temperature was 300°C, the roughness angle significantly increased, and the roughness angles calculated in terms of R_P and Z_S were 12.7824° and 12.9166°, respectively, for a difference of 0.1292°. When the temperature reached 600°C, the calculated values were 20.0512° and 20.3715°, for a difference of 0.3203°. As the temperature changed, the roughness angle calculated with R_P was always smaller than that calculated with Z_S; this pattern became starker as the temperature increased.

An examination of the effect of the water temperature on the roughness angle of the specimen split surface revealed that at a water temperature of 1°C, the roughness angles calculated using R_P and Z_S were approximately 12.4181° and 12.5517°, respectively, for a difference of 0.1336°. At a water temperature of 80°C, the calculated values were 9.5056° and 9.5571°, for a difference of 0.0515°. The lower the water temperature, the higher the roughness angle of the specimen, and the larger the roughness angle difference calculated by R_p and Z_s.

The effect of the number of heating-cooling cycles performed on the roughness angle of the specimen split surface was examined last. As the number of water injection cycles increased, the roughness angle increased. The roughness angles calculated using R_P and Z_S after five cycles were 15.2228° and 16.2101°, respectively, which was the greatest difference between the two methods.

When studying the effect of fracture texture parameters on the heat transfer efficiency, the significance of the variation in the texture parameters for the heat transfer process should be understood. When the texture parameters become more extreme, the effective heat exchange area increases, and the fluid flow carries more heat to improve the thermal

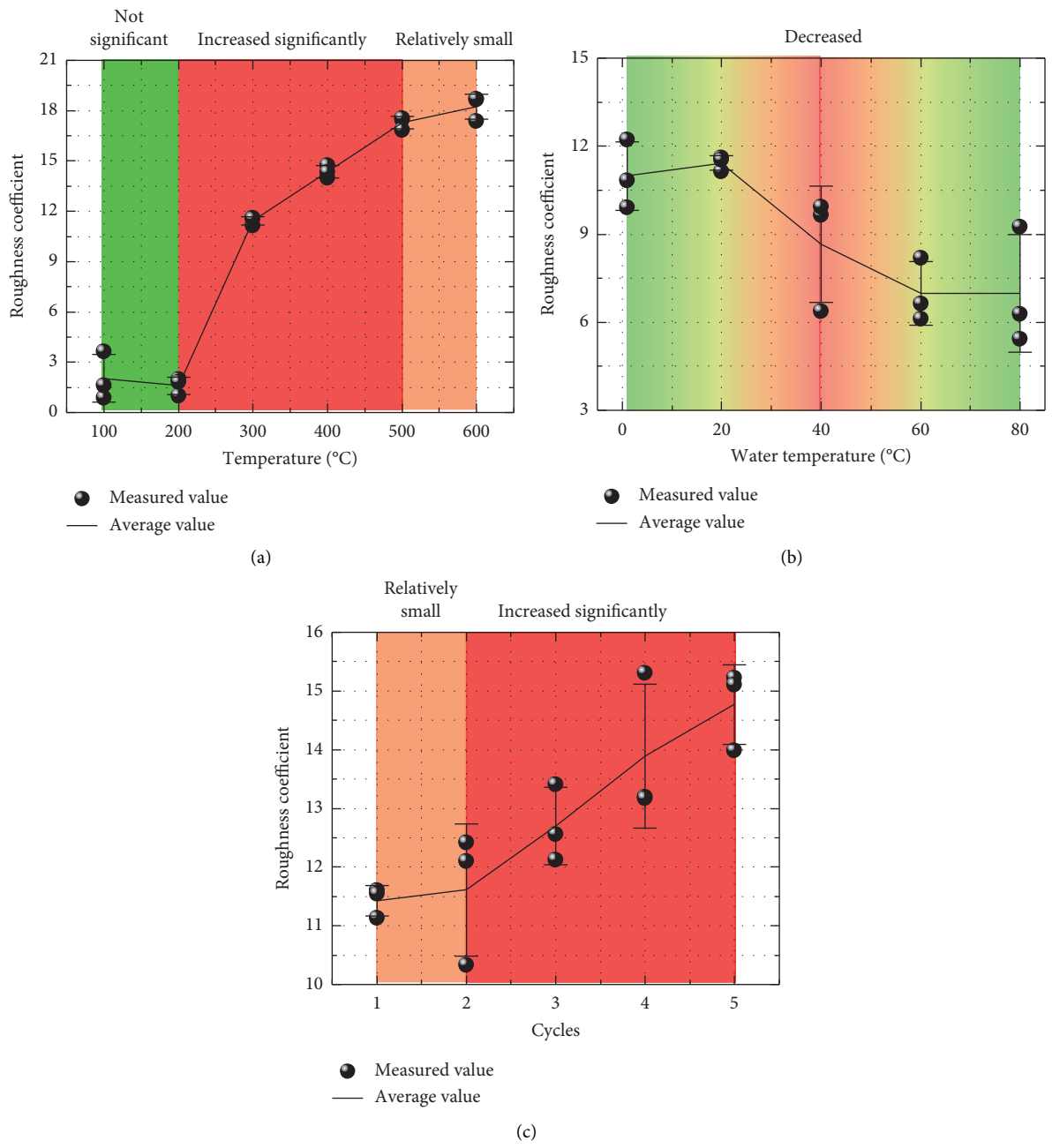

Figure 9: Roughness coefficient of the split surface of specimens under different conditions of water cooling at high temperatures. (a) HDR temperature. (b) Water temperature. (c) The number of heating-cooling cycles.

recovery performance. The different conditions of water cooling at high temperature are important factors in the texture parameters of the split surface. The texture parameters continuously increased as the temperature increased, the cycle number increased, or the water temperature decreased. Therefore, studying the effect of different conditions of water cooling at high temperature on the fracture texture parameters is valuable.

3.6. Relationship between the Tensile Strength and Roughness of the Specimens. The morphological parameters of the fracture surface are related to the injection conditions at high temperatures and the stress environment at the time of fracture. Therefore, it is important to establish a relationship between the split surface height MSE, height variation, and tensile strength of the specimen under different water circulation conditions.

Figures 12(a)–12(c) and 13(a)–13(c) show the relationships between the tensile strength and height MSE and between the tensile strength and roughness coefficient under different conditions of water cooling at high temperature, respectively. Under different temperature conditions, different water temperature conditions, and different numbers of water circulation cycles, there are certain correlations between

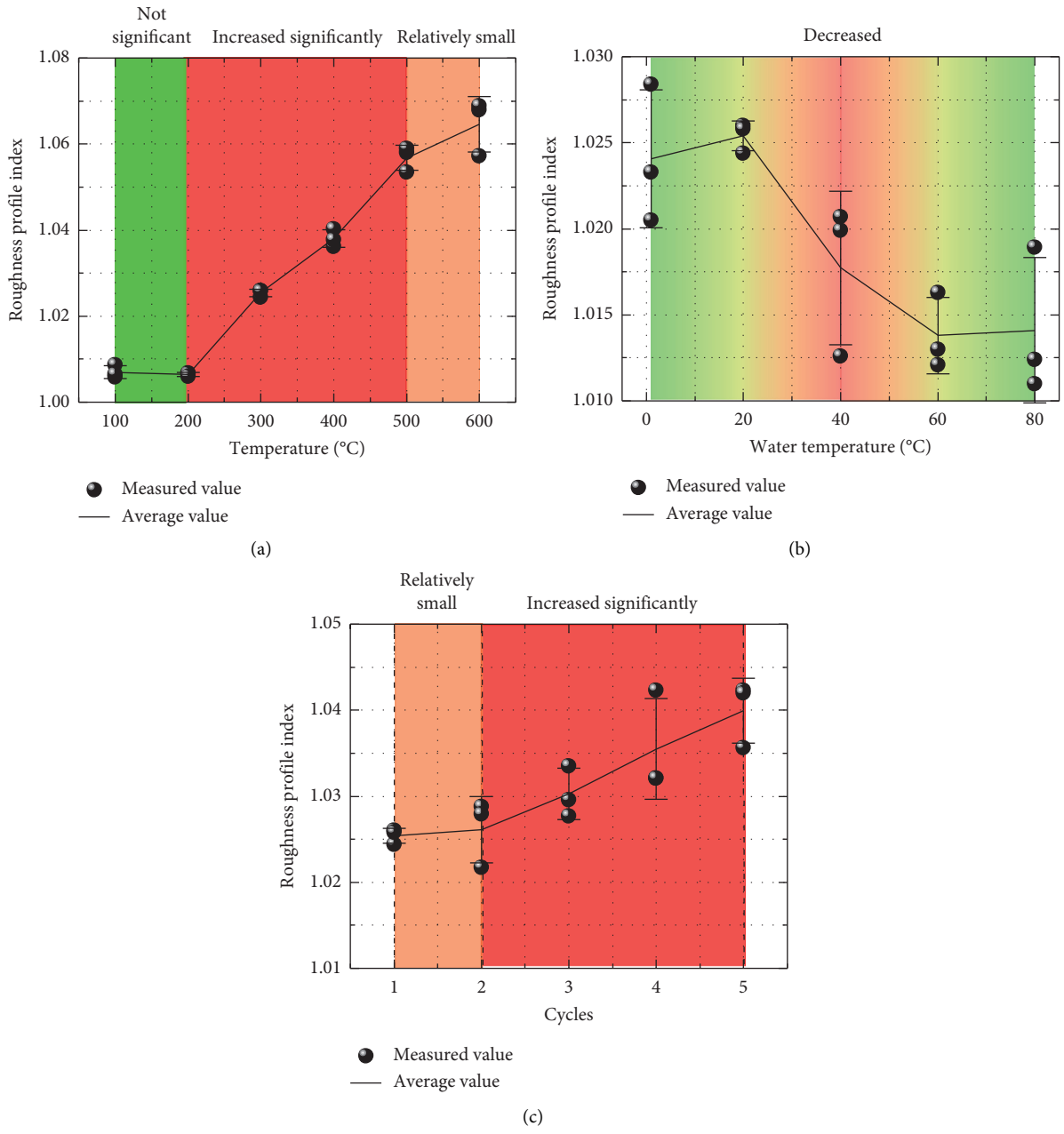

Figure 10: Roughness profile index of the specimen split surface under different conditions of water cooling at high temperatures. (a) HDR temperature. (b) Water temperature. (c) The number of heating-cooling cycles.

the tensile strength and height MSE and between the tensile strength and roughness coefficient. Under the same water temperature and the same number of water circulation cycles but different temperatures, the height MSE and roughness coefficient significantly decreased with the increase in tensile strength. Under same temperature but different water temperatures and different numbers of water circulation cycles, the height MSE and roughness coefficient still decreased with the increase in tensile strength, but the decrease was obviously weaker. The fractures inside the rock have different sizes and states, such as open or closed. Under different fracture states, the tensile strength had a different effect on the specimen, resulting in a different capacity to withstand a splitting load. A high rock body temperature, a low water temperature, and an increasing number of water circulation cycles can all promote the development of fractures inside the rock, aggravating the degree of fracture. The split surface roughness coefficient is the most intuitive index for describing the degree of fracture inside a rock body. The higher the roughness coefficient is, the more severe the fracture, the lower the capability to withstand tensile strength, and vice versa. Temperature changes had the most profound impact on the thermal fracture of the rock, followed by the number of water circulation cycles and the temperature of the injected water. Therefore, it is highly

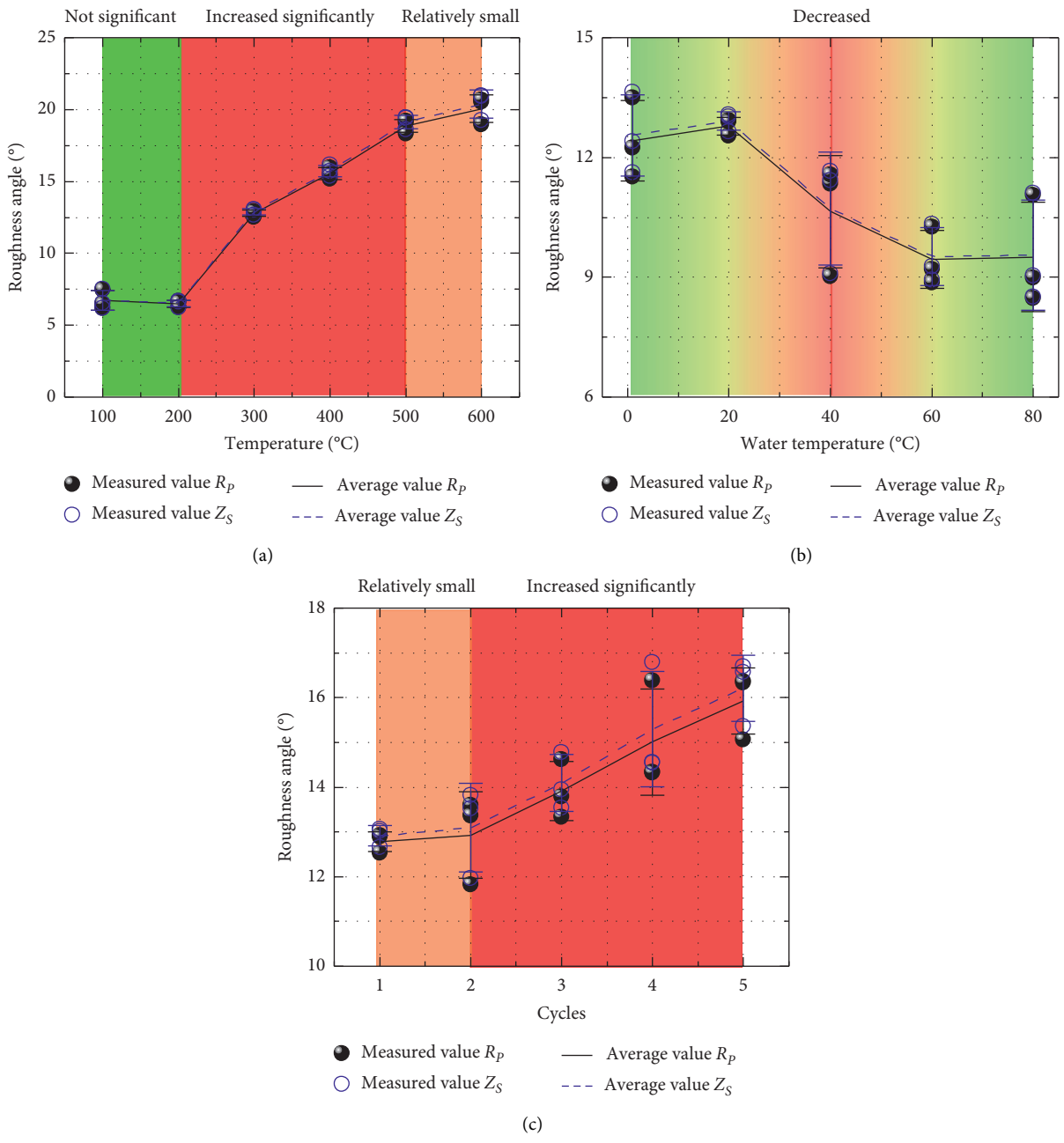

FIGURE 11: Roughness angle of the split surface of the specimen under different conditions of water cooling at high temperatures. (a) HDR temperature. (b) Water temperature. (c) The number of heating-cooling cycles.

feasible to use tensile strength to evaluate the split surface roughness of rock.

3.7. Summary of Test Rules. The rules obtained in this article are summarized, and the conclusions are shown in Table 4.

4. Discussion

The mechanisms related to the physical, mechanical, and split surface roughness characteristics of the granite under different high temperature-cooling conditions are discussed according to the patterns obtained from the tests.

The granite in the target area contains a variety of mineral components, with variations in the content between the components and large differences in the thermal expansion coefficients. Therefore, the mineral components of the rock deform differently under the influence of different high temperature-cooling conditions. The rock as a whole constrains its components to some extent. The part of the rock that expands is compressed, while the part that contracts is elongated. Therefore, an internal force is caused by thermal stress under high temperature conditions. As the temperature rises, the maximum thermal stress usually occurs at the boundary of the rock. When this value is

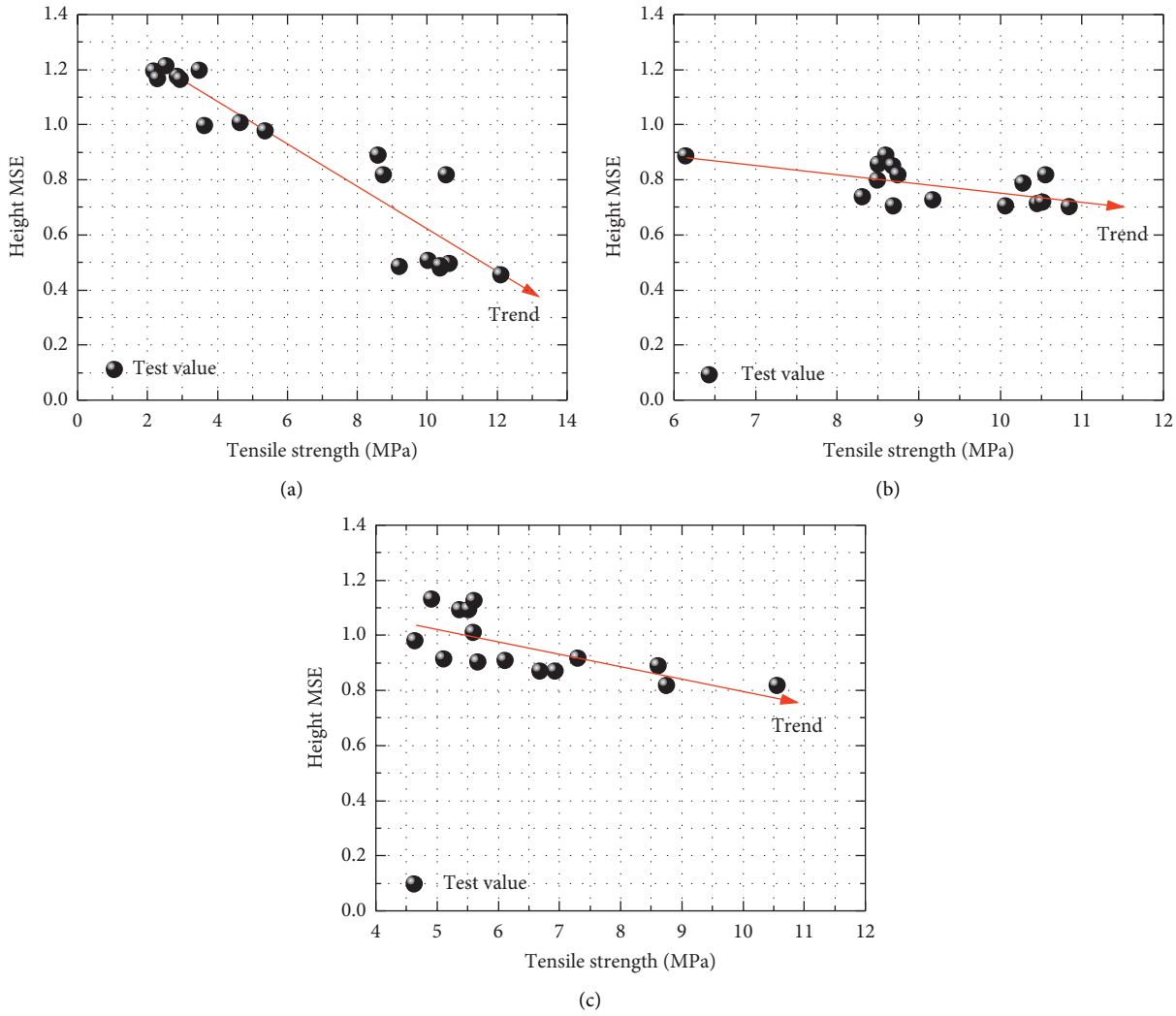

Figure 12: The relationship between the tensile strength and the height MSE. (a) HDR temperature. (b) Water temperature. (c) The number of heating-cooling cycles.

reached or exceeded, fractures occur at the interparticle connections near the boundary and, in turn, form microfractures that propagate into the interior of the rock. The continuous increase in temperature also triggers the phenomenon of thermal stress concentration in some parts of the rock, causing the fractures to extend, intersect, become dense, and coalesce to form a network of microfractures, a phenomenon known as thermal cracking. This process is reflected in the physical and mechanical properties of the rock as the occurrence of fracture and the decay of the mechanical strength, and it is reflected in the split surface as an increase in the roughness.

Water cooling of a rock at high temperatures increases the degree of thermal cracking of the rock. If the high temperature and water cooling processes of the rock are considered as a whole, the water cooling process significantly increases the difference between the temperature fields inside the rock and those at the boundary, which is equivalent to a secondary thermal shock effect on the rock. Thus, the thermal stresses in the rock can be divided into those generated by high temperatures and those formed by the secondary thermal shock of cooling. Assuming that the rock consists of multiple finite units, each of which has only two mineral components, this paper modifies the formula of Zhu et al. [38] and proposes formulas (12)–(15) for the thermal stresses in a process that involves multiple heating-water cooling cycles.

The thermal stresses generated by high temperatures can be calculated as follows:

$$\sigma_{1ij} = \frac{(\gamma_1 - \gamma_2)\Delta T_{1ij} E_1 E_2}{E_1 + E_2}. \tag{12}$$

The thermal stresses generated by the secondary thermal shock of water cooling can be calculated as follows:

$$\sigma_{2ij} = E_{ij}\xi_{ij} = \frac{E_{ij}\gamma_{ij}\Delta T_{2ij}}{1 - 2\mu_{ij}}. \tag{13}$$

The total thermal stresses generated by a single heating-water cooling cycle can be calculated as follows:

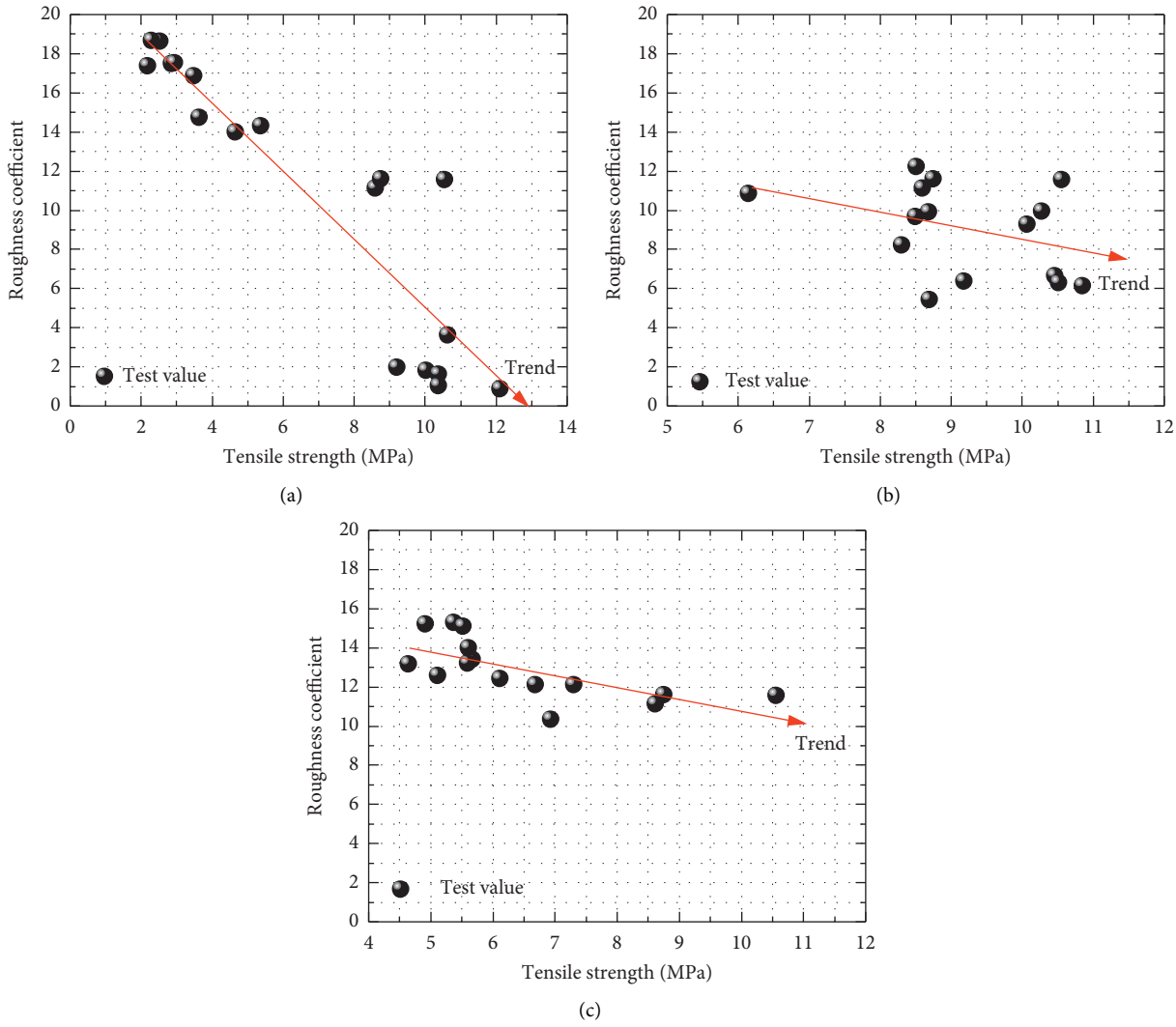

FIGURE 13: The relationship between the tensile strength and the roughness coefficient. (a) HDR temperature. (b) Water temperature. (c) The number of heating-cooling cycles.

$$\sigma_{ij} = \sigma_{1ij} + \sigma_{2ij}. \tag{14}$$

The total thermal stresses generated by multiple heating-water cooling cycles can be calculated as follows:

$$\sigma_{\text{sum}} = \sum_{k=1}^{n} \left(\sigma_{ij}\right)_k, \tag{15}$$

where 1, 2, and ij denote mineral 1, mineral 2, and the ij^{th} unit, respectively; γ_1, γ_2, and γ_{ij} are the volumetric thermal expansion coefficients (1/°C) of mineral 1, mineral 2, and the ij^{th} unit, respectively; ΔT_{1ij} and ΔT_{2ij} are the temperature differences (°C) of the ij^{th} unit caused by high temperatures and the secondary thermal shock of water cooling, respectively; E_1, E_2, and E_{ij} are the elastic moduli (GPa) of mineral 1, mineral 2, and the ij^{th} unit, respectively; μ_{ij} is Poisson's ratio of the ij^{th} unit; n is the number of heating-cooling cycles (taken as 5); and k denotes the k^{th} heating-cooling cycle.

The above formulas indicate that the thermal cracking of a rock is related to the temperature difference of each unit. The larger the temperature difference, the more pronounced the differential expansions of different mineral components of the rock. Therefore, with a higher temperature of the rock and a lower temperature of the water, the temperature difference between the high-temperature rock and the water flow becomes larger to increase the degree of thermal cracking, the roughness of the split surface, and the loss of the tensile strength. In addition, multiple high temperature water cooling cycles further increase the thermal stress generated in the rock, aggravating the degree of thermal cracking.

Our investigation of the specific cooling conditions, with consideration of the above principles and the experimental phenomena, resulted in the following findings. When the temperature was 100–200°C, the thermal cracking stress of the rock was not reached; so, there was no obvious thermal cracking phenomenon, and none of the characteristics of the

Table 4: Summary of test rules.

Influencing factors	Variable interval	Mass loss rate	Tensile strength	Height difference parameters		Texture parameters			Tensile strength and height MSE	Tensile strength and roughness coefficient
				Height MSE	Height fluctuation difference	Roughness coefficient	Roughness profile index	Roughness angle		
Rock temperature	100–200°C	Not significant	Not significant	Not significant	Increased significantly	Not significant	Not significant	Not significant	Decreased significantly	
	200–300°C	Increased significantly	Decreased significantly	Increased significantly		Increased significantly	Increased significantly	Increased significantly		
	300–400°C									
	400–500°C									
	500–600°C	Relatively small	Relatively small	Relatively small	Relatively small	Relatively small	Relatively small			
Maximum	Minimum	100°C	600°C	100°C	100°C	100°C	100°C	100°C		
	600°C	100°C	600°C	600°C	600°C	600°C	600°C			
Water temperature	1–20°C	Decreased	Increased	Decreased	Decreased	Decreased	Decreased	Decreased	Relatively small decrease	
	20–40°C									
	40–60°C									
	60–80°C									
	Minimum	80°C	1°C	80°C	80°C	80°C	80°C	80°C		
	Maximum	1°C	80°C	1°C	1°C	1°C	1°C	1°C		
The number of heating-cooling cycles	1-2 times	Increased significantly	Decreased significantly	Relatively small	Relatively small	Relatively small	Relatively small	Relatively small		
	2-3 times									
	3-4 times	Relatively small	Relatively small	Increased significantly	Increased significantly	Increased significantly	Increased significantly	Increased significantly	Relatively small decrease	
	4-5 times									
	Minimum	1 time	5 times	1 time	1 time	1 time	1 time	1 time		
	Maximum	5 times	1 time	5 times	5 times	5 times	5 times	5 times		

specimen changed significantly. Multiple indices of the 100°C specimen were slightly lower than those of the 200°C specimen, which is speculated to be attributed to the difference of the natural rock itself. The loss of mass of the specimen between 100°C and 200°C was mainly due to the loss of free water. When the rock was heated to 300–400°C, the internal water in the bound form (crystalline water and bound water) underwent a bursting phenomenon (Deng et al. [39]) and was converted to free water, which was then consumed by evaporation, contributing to the loss of mass in the rock and leading to the creation of a large number of microfractures. The influx of external free water into the interior of the rock accelerated the propagation of microfractures. When the rock temperature continued to increase to 500°C, the heating-cooling process significantly increased the temperature difference between the interior and exterior of the rock, leading to an increase in the total thermal stress, which promoted further extension and propagation of the thermal cracking in the rock. As a result, its mechanical properties continued to decrease, the roughness of the split surface continued to increase, and at this point, there was a loss of structural water in the rock. When the temperature reached 600°C, the amplitude of variation in the mechanical indices and the roughness index of the split surface of the specimen decreased because high temperatures also increase the size of pores in rock, and large pores can absorb the energy generated by thermal stress, inhibit the deformation of particles, and thus prevent the formation of cracks to some extent. However, an increase in porosity also leads to a decrease in the ability of a rock to resist thermal cracking. Therefore, the influence of the pore structure on the properties of a rock after high temperature heating is two-sided. Based on observations of the surface of the specimen, when the temperature was between 500°C and 600°C, the edge particles fell off, leading to further loss of the rock mass. In addition, a higher temperature and a larger number of heating-cooling cycles led to a more pronounced degree of thermal cracking of the rock. Meanwhile, microparticles flowed out of the rock with water from the fractures, which is another important factor causing a loss of the specimen mass. The use of high-temperature water injection can inhibit the generation of thermal cracking of the rock and reduce the outflow of microparticles from the pores, thus preventing particles from clogging the fractures and affecting the efficiency of the water-rock heat exchange process.

The heat transfer mode is another important factor that cannot be ignored in HDR development. When the temperature is low, the granite has a dense structure, and the internal heat transfer is dominated by intermatrix heat transfer. As the temperature increases, a large number of fractures appeared in the rock, and consequently, the heat transfer process of the rock is affected by both intermatrix heat transfer and matrix-water thermal convection. The test results show that when the water temperature was close to 1°C, there was an abnormal phenomenon that the roughness index of the split surface of each group of specimens was lower than that at a water temperature of 20°C. This is because during the cooling process, ice cubes were continuously added to the water to ensure that the water temperature was close to 1°C. This practice increased the dynamic viscosity of the water, leading to a significant decrease in the flow rate of water in the fractures, inhibiting the flow path of water in the rock, reducing the area of heat exchange between the rock and the water, and eventually resulting in a decrease in the degree of cracking of the rock and a relatively small roughness index of the split surface.

The variation in mineral parameters in the rock under high temperature water cooling was also a factor to be considered. At room temperature, the interior of the rock is mainly composed of quartz, mica, potash feldspar, plagioclase, pyroxene, and hornblende, with the contents of quartz, mica, and feldspar accounting for approximately 96%. Therefore, the granite in its natural state is greyish white, with black spots, i.e., biotite. When the temperature increased to 300–400°C, the quartz crystal burst and the crystal state changed; the colour changed from transparent to white, so the rock also changed from greyish white to white, while the biotite lost crystalline water under high temperature conditions, so the number of black spots of the specimen was greatly reduced. When the rock was heated to 500°C, the ferrous ions in the ferrous oxides contained in plagioclase were converted to ferric ions, causing some areas of the specimen to appear reddish brown. When the temperature continued to rise to 600°C, the specimen surface turned blackish grey because the surface changed from smooth to rough, and the presence of white crystals was due to the repetitive phase change of the quartz at 573°C (Shen et al. [40]). The multiple high temperature water cooling cycles reduced the temperature of quartz crystal bursting. Therefore, the variation pattern of mineral parameters in the rock can be determined by the change in the appearance characteristics of the specimen.

In summary, the high temperature-cooling conditions affect the HDR development to some extent by notably changing the physicomechanical properties, thermal cracking morphology, and fracture surface roughness characteristics of the rock. How to fracture rock and use the rough surface of fractures for water flow and heat transfer will be the focus of future research.

5. Conclusions

This was an experimental study of the physical and mechanical properties and the split surface roughness characteristics of granite after water cooling at high temperatures under different conditions of water cooling at high temperature. The following conclusions can be drawn.

(1) When the rock temperature rose, the water temperature dropped or the number of heating-cooling cycles increased and the mass loss rate of the specimen increased. The rise in the temperature and the increase in the number of water cooling cycles changed the appearance (colour) of the specimen. Therefore, different conditions of water cooling at high temperature experienced by the thermal

recovery area can be deduced from changes in the appearance characteristics.

(2) By increasing the rock temperature, increasing the number of heating-cooling cycles, or decreasing water injection temperature, the mechanical properties of the specimen became weaker, and the values of the roughness gradually increased. The different conditions of water cooling at high temperature that influenced the physical and mechanical properties and the roughness characteristics of the rock in the thermal recovery area, from most to least important, were the temperature of the target area, the number of water injection cycles, and the water injection temperature. By selecting high-temperature reservoirs as the target areas for drilling and adopting low-temperature water injection and multiple cold-water circulation cycles, rock strata can be fractured to improve the permeability of reservoirs.

(3) Under different water cooling conditions, the tensile strength was negatively correlated with the roughness index. When the tensile strength changes, the impact on the roughness was in the descending order of the target area temperature, the number of water circulation cycles, and the water temperature. Thus, tensile strength can be used as an indicator for evaluating the surface roughness under different conditions of water cooling at high temperature.

Data Availability

The data used to support the findings of this study are available from the corresponding author upon request.

Conflicts of Interest

The authors declare that there are no conflicts of interest.

Acknowledgments

This research was supported by the National Natural Science Foundation of China (51874165), the Liaoning Province "Xingliao Talent Program" (XLYC1902106), and the National Key R&D Program of China (2016YFC0600901).

References

[1] MIT, *The Future of Geothermal Energy-Impact of Enhanced Geothermal Systems (EGS) on the United States in the 21st Century, An Assessment by an MIT-Led Interdisciplinary Panel*, Massachusetts Institute of Technology, Boston, MA, USA, 2006.

[2] Y. Jing, Z. Jing, J. Willis-Richards, and T. Hashida, "A simple 3-D thermoelastic model for assessment of the long-term performance of the Hijiori deep geothermal reservoir," *Journal of Volcanology and Geothermal Research*, vol. 269, pp. 14–22, 2014.

[3] C. Vogt, G. Marquart, C. Kosack, A. Wolf, and C. Clauser, "Estimating the permeability distribution and its uncertainty at the EGS demonstration reservoir Soultz-sous-Forts using the ensemble Kalman filter," *Water Resources Research*, vol. 48, no. 8, pp. 8517–8531, 2012.

[4] Y. Zhao, Z. Wan, and J. Kang, *Introduction to Geothermal Development of High Temperature Rock Mass*, Science Press, Beijing, China, 2004.

[5] Y. Xin, L. Zhuang, and Z. Sun, "Numerical investigation on the effects of the fracture network pattern on the heat extraction capacity for dual horizontal wells in enhanced geothermal systems," *Geomechanics and Geophysics for Geo-Energy and Geo-Resources*, vol. 6, no. 2, pp. 533–552, 2020.

[6] D. B. Fox, D. Sutter, K. F. Beckers et al., "Sustainable heat farming: modeling extraction and recovery in discretely fractured geothermal reservoirs," *Geothermics*, vol. 46, pp. 42–54, 2013.

[7] A. Kazemi, S. Mahbaz, A. Dehghani-Sanij, M. Dusseault, and R. Fraser, "Performance evaluation of an enhanced geothermal system in the Western Canada sedimentary basin," *Renewable and Sustainable Energy Reviews*, vol. 113, Article ID 109278, 2019.

[8] A. Battaillé, P. Genthon, M. Rabinowicz, and B. Fritz, "Modeling the coupling between free and forced convection in a vertical permeable slot: implications for the heat production of an enhanced geothermal system," *Geothermics*, vol. 35, no. 5-6, pp. 654–682, 2006.

[9] B. Gong, H. Liang, S. Xin, and K. Li, "Effect of water injection on reservoir temperature during power generation in oil fields," in *Proceedings of the 36th Workshop on Geothermal Reservoir Engineering*, Stanford, CA, USA, January 2011.

[10] P. K. Gautam, A. K. Verma, M. K. Jha, P. Sharma, and T. N. Singh, "Effect of high temperature on physical and mechanical properties of Jalore granite," *Journal of Applied Geophysics*, vol. 159, pp. 460–474, 2018.

[11] Y. Shen, X. Hou, J. Yuan, and C. Zhao, "Experimental study on temperature change and crack expansion of high temperature granite under different cooling shock treatments," *Energies*, vol. 12, no. 11, 2019.

[12] Y. Shen, X. Hou, J. Yuan et al., "Thermal deterioration of high-temperature granite after cooling shock: multiple-identification and damage mechanism," *Bulletin of Engineering Geology and the Environment*, vol. 7, pp. 1–14, 2020.

[13] X. Hu, X. Song, Y. Liu, Z. Cheng, J. Ji, and Z. Shen, "Experiment investigation of granite damage under the high-temperature and high-pressure supercritical water condition," *Journal of Petroleum Science and Engineering*, vol. 180, pp. 289–297, 2019.

[14] B. Isaka, R. Gamage, T. Rathnaweera, M. Perera, D. Chandrasekharam, and W. Kumari, "An influence of thermally-induced micro-cracking under cooling treatments: mechanical characteristics of Australian granite," *Energies*, vol. 11, no. 6, 2018.

[15] Z. Zhao, "Thermal influence on mechanical properties of granite: a microcracking perspective," *Rock Mechanics and Rock Engineering*, vol. 49, no. 3, pp. 747–762, 2015.

[16] B. Li and F. Ju, "Thermal stability of granite for high temperature thermal energy storage in concentrating solar power plants," *Applied Thermal Engineering*, vol. 138, pp. 409–416, 2018.

[17] M. Hosseini, "Effect of temperature as well as heating and cooling cycles on rock properties," *Journal of Mining and Environment*, vol. 8, no. 4, pp. 631–644, 2017.

[18] T. Ficker, "Rock joint coefficients and their computerized classification," *International Journal of Mining Science and Technology*, vol. 29, no. 5, pp. 701–709, 2019.

[19] L. Zeng, J. Qi, and Y. Wang, "Origin type of tectonic fractures and geological conditions in low-permeability reservoirs," *Acta Petrolei Sinica*, vol. 28, no. 4, pp. 52–56, 2007.
[20] G. Grasselli and P. Egger, "Constitutive law for the shear strength of rock joints based on three-dimensional surface parameters," *International Journal of Rock Mechanics and Mining Sciences*, vol. 40, no. 1, pp. 25–40, 2003.
[21] W. Zhang, Q. Sun, S. Hao, J. Geng, and C. Lv, "Experimental study on the variation of physical and mechanical properties of rock after high temperature treatment," *Applied Thermal Engineering*, vol. 98, pp. 1297–1304, 2016.
[22] M. Diaz, K. Y. Kim, S. Yeom, L. Zhuang, S. Park, and K.-B. Min, "Surface roughness characterization of open and closed rock joints in deep cores using X-ray computed tomography," *International Journal of Rock Mechanics and Mining Sciences*, vol. 98, pp. 10–19, 2017.
[23] Z. C. Tang and Y. Zhang, "Temperature-dependent peak shear-strength criterion for granite fractures," *Engineering Geology*, vol. 269, p. 105552, 2020.
[24] R. Li, Z. Huang, X. Wu, P. Yan, and X. Dai, "Cryogenic quenching of rock using liquid nitrogen as a coolant: investigation of surface effects," *International Journal of Heat and Mass Transfer*, vol. 119, pp. 446–459, 2018.
[25] Z. C. Tang, "Experimental investigation on temperature-dependent shear behaviors of granite discontinuity," *Rock Mechanics and Rock Engineering*, vol. 53, no. 9, pp. 4043–4060, 2020.
[26] Z. C. Tang, Q. Z. Zhang, and J. Peng, "Effect of thermal treatment on the basic friction angle of rock joint," *Rock Mechanics and Rock Engineering*, vol. 53, no. 4, pp. 1973–1990, 2020.
[27] Z. Tang and Y. Jiao, "Choosing appropriate appraisal to describe peak-spatial features of rock-joint profiles," *International Journal of Geomechanics*, vol. 20, no. 4, Article ID 04020021, 2020.
[28] C. Zhang, S. Zhang, S. Li et al., "Geothermal characteristics of the Qiabuqia geothermal area in the Gonghe basin, Northeastern Tibetan Plateau," *Chinese Journal of Geophysics-Chinese Edition*, vol. 61, no. 11, pp. 4545–4557, 2018.
[29] Y. Li, "Preliminary study on EGS geothermal resources evaluation and exploration in Song-Liao basin," Master thesis, Jilin University, Changchun, China, 2017.
[30] F. Zhang, J. Zhao, D. Hu, F. Skoczylas, and J. Shao, "Laboratory investigation on physical and mechanical properties of granite after heating and water-cooling treatment," *Rock Mechanics and Rock Engineering*, vol. 51, no. 3, pp. 677–694, 2017.
[31] Y. Zhao, Z. Feng, Y. Zhao, and Z. Wan, "Experimental investigation on thermal cracking, permeability under HTHP and application for geothermal mining of HDR," *Energy*, vol. 132, pp. 305–314, 2017.
[32] W. Zhang, T.-K. Guo, Z.-Q. Qu, and Z. Wang, "Research of fracture initiation and propagation in HDR fracturing under thermal stress from meso-damage perspective," *Energy*, vol. 178, pp. 508–521, 2019.
[33] R. Yang, Z. Huang, Y. Shi, Z. Yang, and P. Huang, "Laboratory investigation on cryogenic fracturing of hot dry rock under triaxial-confining stresses," *Geothermics*, vol. 79, pp. 46–60, 2019.
[34] Ministry of Land and Resources of the People's Republic of China, *DZ/T 0276-2015 Regulation For Testing the Physical and Mechanical Properties of Rock*, Standards Press of China, Beijing, China, 2015.
[35] Z. Yan, H. Zhu, T. Deng, L. Zeng, J. Yao, and J. Qiang, "Experimental study on longitudinal wave characteristics of tuff, granite and breccia after high temperature," *Chinese Journal of Geotechnical Engineering*, vol. 28, no. 11, pp. 2010–2014, 2016.
[36] B. Xi and Y. Zhao, "Experimental research on mechanical properties of water-cooled granite under high temperatures within 600°C," *Chinese Journal of Rock Mechanics and Engineering*, vol. 29, no. 5, pp. 892–898, 2010.
[37] N. Barton, "Review of a new shear-strength criterion for rock joints," *Engineering Geology*, vol. 7, no. 4, pp. 287–332, 1973.
[38] Y. Zhu, J. Yu, H. Gao, G. Li, X. Zhou, and X. Zheng, "Effect of water cooling on microscopic damage and dynamic properties of high-temperature granite," *Explosion and Shock Waves*, vol. 39, no. 8, pp. 1–12, 2019.
[39] L. Deng, X. Li, Y. Wu et al., "Study on mechanical damage characteristics of granite with different cooling methods," *Journal of China Coal Society*, 2020.
[40] Y. Shen, X. Hou, J. Yuan, S. Wang, and C. Zhao, "Thermal cracking characteristics of high temperature granite suffering from different cooling shocks," *International Journal of Fracture*, vol. 225, pp. 153–168, 2020.